

Univerzita Karlova v Praze
Matematicko-fyzikální fakulta
Katedra fyziky nízkých teplot

JAROSLAVA ČERNÁ

NMR IMAGING
DEMONSTRACE ZÁKLADNÍCH PRINCIPŮ

Autoreferát doktorské disertační práce

Praha 2006

Charles University in Prague
Faculty of Mathematics and Physics
Department of Low Temperature Physics

JAROSLAVA ČERNÁ

NMR IMAGING
DEMONSTRATION OF BASIC PRINCIPLES

Summary of PhD Thesis

Prague 2006

Výsledky tvořící disertační práci byly získány během doktorského studia na Matematicko-fyzikální fakultě Univerzity Karlovy v letech 2002–2006.

Doktorand: Mgr. Jaroslava Černá

Školitel: Prof. RNDr. Jiří Englich, DrSc.
Katedra fyziky nízkých teplot MFF UK
V Holešovičkách 2, Praha 8

Školící pracoviště: Katedra fyziky nízkých teplot MFF UK
V Holešovičkách 2, Praha 8

Předseda oborové rady: Doc. RNDr. Jiří Langer, CSc.
Ústav teoretické fyziky MFF UK
V Holešovičkách 2, Praha 8

Oponenti: Ing. Richard Hrabal, CSc.
Laboratoř NMR spektroskopie
Vysoká škola chemicko-technologická
Technická 5, 166 28 Praha 6

Ing. Jaroslav Tintěra, CSc.
Oddělení magnetické rezonance – spektroskopie
Institut klinické a experimentální medicíny
Václavská 1958/9, 140 21 Praha 4

Autoreferát byl rozeslán dne: 18. 8. 2006

Obhajoba se koná dne 18. 9. 2006 v 10:00 hodin před komisí pro obhajoby disertačních prací v oboru F 12 – Obecné otázky fyziky na MFF UK, V Holešovičkách 2, Praha 8, v seminární místnosti Katedry didaktiky fyziky – A 804.

S disertační prací je možno se seznámit na útvaru doktorského studia MFF UK, Ke Karlovu 3, Praha 2.

<i>CONTENTS</i>	4
-----------------	---

Contents

Introduction	5
1 NMR Imaging	5
1.1 Frequency encoding	5
1.2 Back projection	6
1.3 Contrast	7
2 Experimental part	8
2.1 Gradient coil	8
2.2 NMR spectra in the gradient magnetic field	12
2.3 ρ -, T_1 - and T_2 -weighted images	14
Conclusion	17
List of publications	18
References	19

Introduction

The nuclear magnetic resonance imaging (NMR imaging) enables to determine the spatial structure of measured objects. It is nowadays used especially in medicine since it produces a clear anatomical display with good tissue discrimination and with no radiation risk to patients.

The aim of my thesis was to prepare a new experiment for the student laboratory. This experiment should demonstrate the basic principles of the NMR imaging and allow students to familiarize with this very useful experimental method.

1 NMR Imaging

1.1 Frequency encoding

The main principle behind the magnetic resonance imaging is the resonance condition

$$\omega_0 = \gamma B_0 \quad (1)$$

giving the linear dependence between the resonance frequency ω_0 of a magnetic moment and the strength of the magnetic field B_0 at the location of this moment. The resonance frequency can be determined from the measured signal using the Fourier transformation.

Let us illustrate the principle of the NMR imaging on a simple example. Consider a sample that is divided into three separated regions as in Figure 1. In the homogeneous magnetic field there is only one peak at the frequency $\omega_0 = \gamma B_0$ in the NMR spectrum. If a magnetic field with a constant gradient,

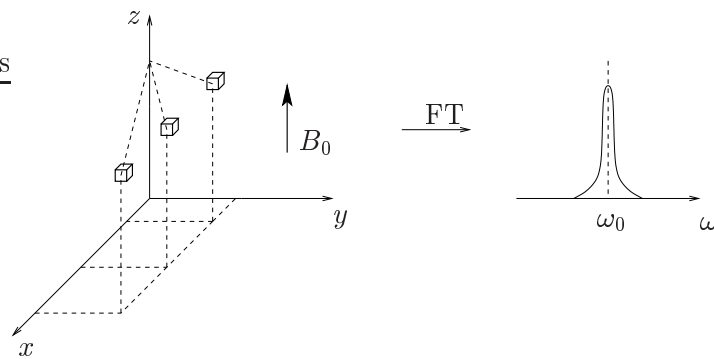


Fig. 1: NMR spectrum in the homogeneous field B_0 . The spectrum contains one peak at the frequency $\omega_0 = \gamma B_0$.

$G_x^z = \frac{\partial B_z}{\partial x} = \text{const.}$, is applied in conjunction with B_0 (Figure 2), then the three regions experience different magnetic fields. The result is an NMR spectrum

with three signals. Their frequencies correspond to the positions of individual regions of the sample in the x direction,

$$\omega_0(x) = \gamma \left(B_0 + \frac{\partial B_z}{\partial x} \cdot x \right). \quad (2)$$

The amplitudes of the signals are proportional to the number of spins in each region of the sample. The described procedure is called the frequency encoding.

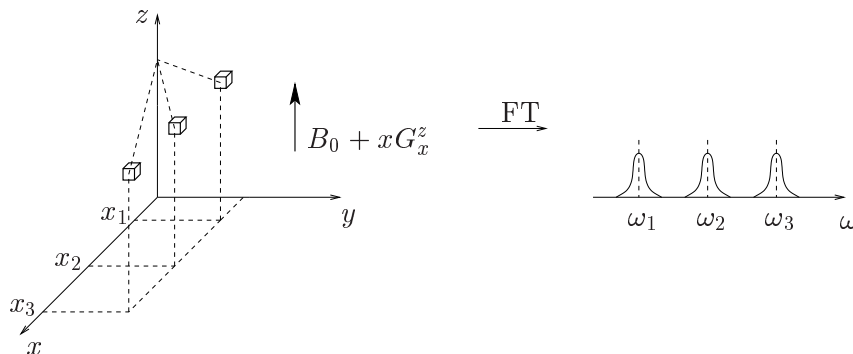


Fig. 2: NMR spectrum in the gradient field $B_0 + xG_x^z$. Resonance frequencies $\omega_1, \omega_2, \omega_3$ correspond to the positions x_1, x_2, x_3 of sample regions.

1.2 Back projection

The back projection is an extension of the frequency-encoding procedure that is used for more complicated samples. For such samples the application of a magnetic-field gradient in one direction only does not give enough information to reconstruct the shape of the sample. This problem can be solved by applying the gradient in several different directions. The shape of the sample can be then deduced from all recorded spectra (see Figure 3).

The method of rotating gradient described above can be equivalently replaced by the method of rotating sample. The technical realization of the latter is easier since the presence of a stationary magnetic-field gradient in one direction is only required. Therefore this method was chosen in our experimental setup.

In the back-projection method we measure a set of spectra for n different angles between the sample and the magnetic-field gradient. The angles stretch from 0° to 180° with the step size δ . The measured spectra are then processed in the following way. First, all spectra are projected into gray-level images: The maximum value is found among amplitudes in the set of measured NMR spectra. White color is assigned to this maximum, shades of gray

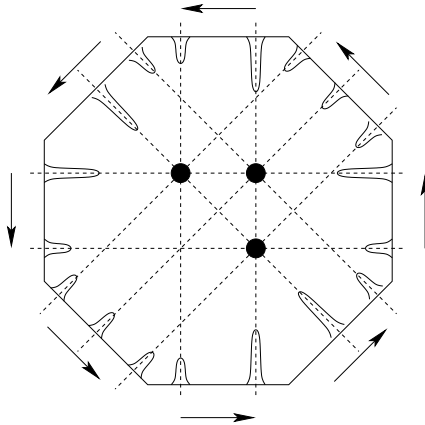


Fig. 3: Back projection: By using field gradients at several angles the positions of the spin-containing regions can be determined.

are assigned to other values. One measured spectrum and the assigned projection is shown in Figure 4. All grey-level projections can be then processed mathematically in order to recover the shape of the sample.

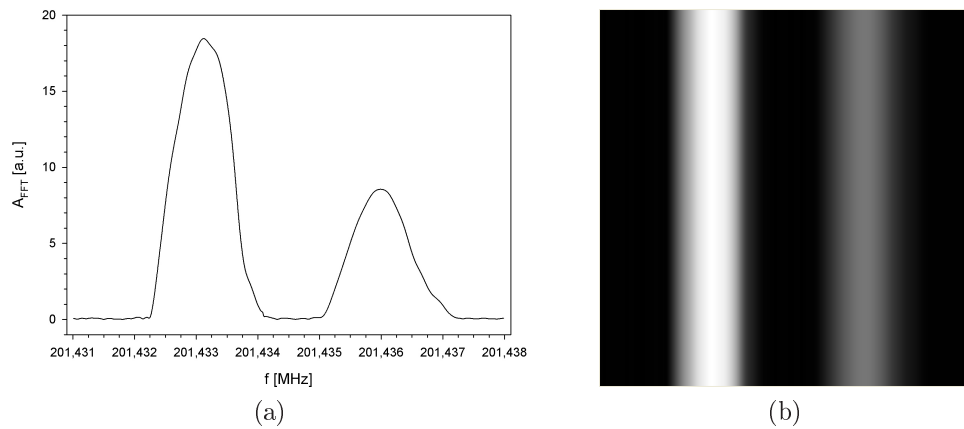


Fig. 4: Assignment of the NMR spectrum (a) and its projection (b).

1.3 Contrast

In order to distinguish various substances contained in the sample, the intensities of the signals originating from them should differ. The relative difference between the areas of the high signal intensity and the low signal intensity is referred to as contrast. Images obtain principal contrast through the difference in proton densities. Results of imaging depending only on different proton densities are called ρ -weighted images. However, the proton density can be almost

constant in many cases and the contrast of the resulting image is then insufficient. An improvement of the contrast can be achieved by using differences in spin-lattice relaxation times T_1 and spin-spin relaxation times T_2 of different substances in the sample. T_1 -, T_2 - or ρ -weighted images can be obtained by applying a convenient pulse sequence, which is a set of RF pulses applied to the sample to produce a specific form of the NMR signal.

Contrast that depends on different spin-lattice relaxation times T_1 can be obtained e.g. by use of the inversion recovery pulse sequence. Assume that the sample contains two substances A and B . Signal intensity behavior of these substances is shown in Figure 5a. Figure 5b depicts the time dependence of the difference of signal intensities $M_z^A - M_z^B$. The difference reaches a maximum

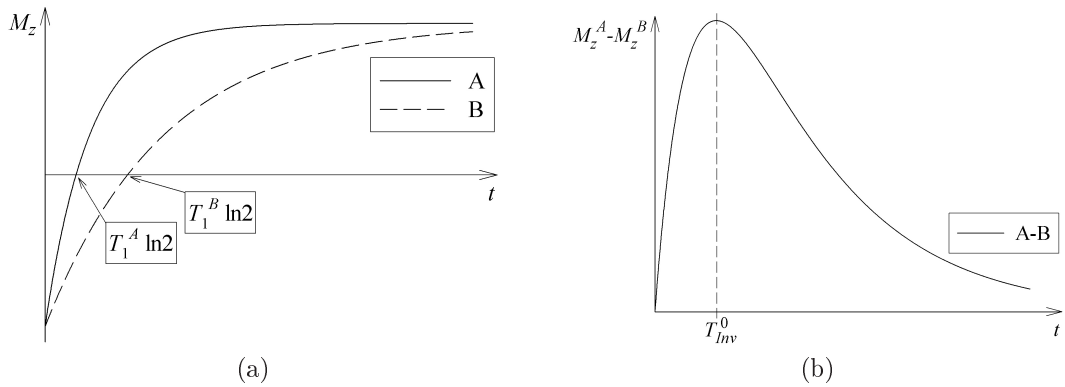


Fig. 5: (a) Signal intensity behavior of substances A and B when the inversion recovery pulse sequence is applied. (b) Time dependence of the difference of signal intensities $M_z^A - M_z^B$.

at T_{Inv}^0 . Therefore, to obtain the optimal contrast we have to set the parameter T_{Inv} (the delay between the 180° excitation pulse and the 90° excitation pulse) to the value of T_{Inv}^0 . If T_{Inv} is set to the value $T_1^A \ln 2$ or $T_1^B \ln 2$, the signal from substance A or B totally disappears.

A T_2 -weighted image can be created by applying the spin echo pulse sequence. Signal decay curves and the difference of signal intensities of substances A and B are shown in Figure 6. The difference reaches the maximum value at T_E^0 . When we set the delay between the 90° excitation pulse and the 180° excitation pulse to $\frac{1}{2}T_E^0$ contrast of the created image is the best.

2 Experimental part

2.1 Gradient coil

To reconstruct the spatial structure of a measured sample the presence of a magnetic-field gradient is essential. The method of the back projection with

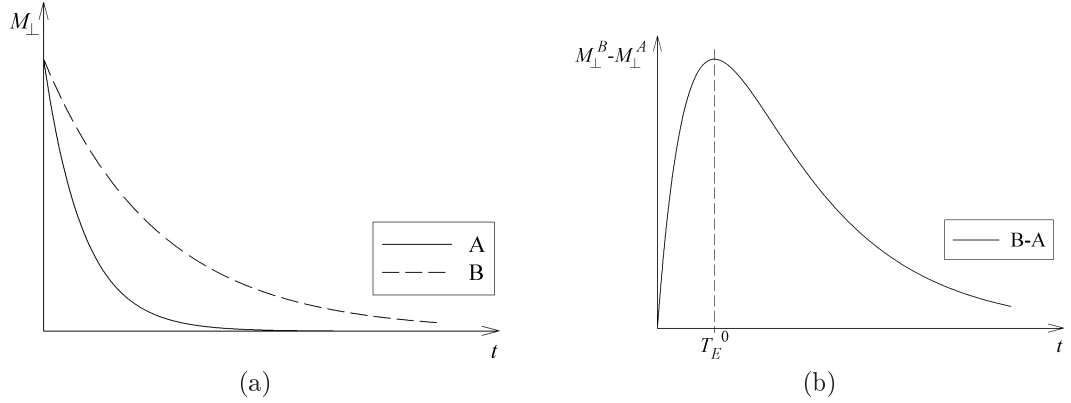


Fig. 6: (a) Signal decay curves of substances A and B when the spin echo pulse sequence is applied. (b) Time dependence of the difference of signal intensities $M_{\perp}^B - M_{\perp}^A$.

rotating sample, which is used in our experimental setup, requires a stationary gradient in one direction (e.g. x). A magnetic field with the constant gradient $\frac{\partial B_z}{\partial x}$ can be produced by a special saddle coil placed on a cylindrical surface. The main design problem is to optimize the position of conductors in the coil and the current flowing through them to achieve an optimal form of the magnetic-field gradient.

The basic element of the coil is a circular arc (Figure 7a), which is located in a plane perpendicular to the z -axis. Its induction component B_z at the point

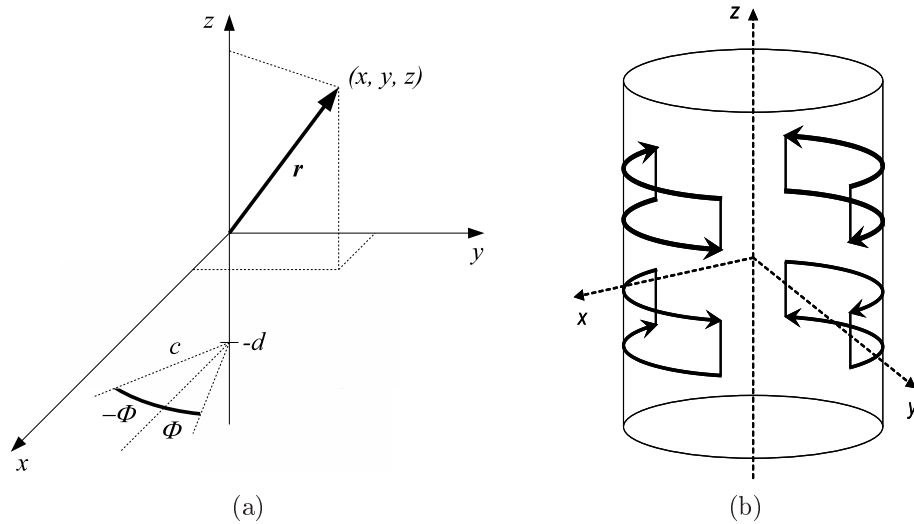


Fig. 7: (a) Coordinates for the computation of the magnetic field of a conductor in the form of a circular arc. (b) Saddle coils producing the gradient in the x -direction.

(x, y, z) is given by the Biot-Savart law

$$B_z(x, y, z) = \frac{\mu I c}{4\pi} \int_{-\Phi}^{\Phi} \frac{(c - x \cos \xi - y \sin \xi) d\xi}{[x^2 + y^2 + (z + d)^2 - 2c(x \cos \xi + y \sin \xi) + c^2]^{\frac{3}{2}}}, \quad (3)$$

where I is the current flowing through the circular arc of radius c and opening angle 2Φ , d is the z -coordinate of the plane in which the arc lies and μ is the permeability.

Eq. (3) can be simplified by the use of the relative coordinates

$$X = \frac{x}{c}, \quad Y = \frac{y}{c}, \quad Z = \frac{z}{c}$$

to the formula

$$B_z(X, Y, Z) = B_z^0 \int_{-\Phi}^{\Phi} \frac{(1 - X \cos \xi - Y \sin \xi) d\xi}{[X^2 + Y^2 + (Z + \beta)^2 - 2(X \cos \xi + Y \sin \xi) + 1]^{\frac{3}{2}}}, \quad (4)$$

where

$$B_z^0 = \frac{\mu I}{4\pi c} \quad \text{and} \quad \beta = \frac{d}{c}. \quad (5)$$

An ideal x -gradient coil produces a magnetic field with a constant gradient along the x -axis. The simplest type consists of four symmetrically positioned saddle coils placed on a cylinder, as shown in Figure 7b. It contains eight basic arcs.

The magnetic field B_z (Eq. (4)) in the neighbourhood of the origin can be approximated by the three-dimensional Taylor series

$$B_z(X, Y, Z) = \sum_{i,j,k=0}^{\infty} \tau_{i,j,k} X^i Y^j Z^k, \quad (6)$$

where

$$\tau_{i,j,k} = \frac{1}{i! j! k!} \left. \frac{\partial^{i+j+k} B_z(X, Y, Z)}{\partial X^i \partial Y^j \partial Z^k} \right|_{X=Y=Z=0}. \quad (7)$$

As it is shown in the thesis, the only nonzero derivative of the first order is (in the configuration according to Figure 7b)

$$\left. \frac{\partial B_z}{\partial X} \right|_0 = 2B_z^0 \frac{(2 - \beta^2) \sin \Phi}{(\beta^2 + 1)^{\frac{5}{2}}}, \quad (8)$$

The nonzero derivatives of the second order are

$$\left. \frac{\partial^2 B_z}{\partial X^2} \right|_0 = \frac{3}{2} B_z^0 \frac{2(1 - 4\beta^2)\Phi - (2\beta^2 - 3) \sin(2\Phi)}{(\beta^2 + 1)^{\frac{7}{2}}}, \quad (9)$$

$$\left. \frac{\partial^2 B_z}{\partial Y^2} \right|_0 = \frac{3}{2} B_z^0 \frac{2(1 - 4\beta^2)\Phi + (2\beta^2 - 3) \sin(2\Phi)}{(\beta^2 + 1)^{\frac{7}{2}}}, \quad (10)$$

and finally the nonzero derivatives of the third order are

$$\left. \frac{\partial^3 B_z}{\partial X \partial Y^2} \right|_0 = \frac{1}{2} B_z^0 \frac{3(4\beta^4 - 27\beta^2 + 4) \sin \Phi + 5(3\beta^2 - 4) \sin(3\Phi)}{(\beta^2 + 1)^{\frac{9}{2}}}, \quad (11)$$

$$\left. \frac{\partial^3 B_z}{\partial X \partial Z^2} \right|_0 = -6 B_z^0 \frac{(4\beta^4 - 27\beta^2 + 4) \sin \Phi}{(\beta^2 + 1)^{\frac{9}{2}}}, \quad (12)$$

$$\left. \frac{\partial^3 B_z}{\partial X^3} \right|_0 = \frac{1}{2} B_z^0 \frac{9(4\beta^4 - 27\beta^2 + 4) \sin \Phi - 5(3\beta^2 - 4) \sin(3\Phi)}{(\beta^2 + 1)^{\frac{9}{2}}}. \quad (13)$$

To design an x -gradient coil we have to maximize the term (8) and to minimize the undesirable terms (9)–(13) by a suitable choice of the parameters c , d and Φ .

To increase the size of the gradient, which is produced by the simplest type of the x -gradient coil (Figure 7b), a coil with more turns and layers can be used. We used the x -gradient coil consisting of four turns and two layers (Figure 8).

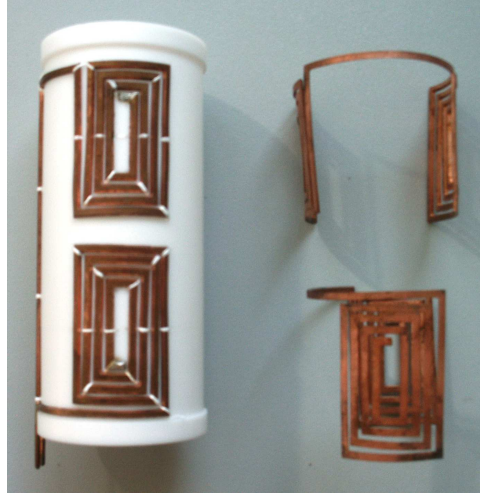


Fig. 8: Realization of the x -gradient coil.

To test the homogeneity of the gradient, the magnetic field B_z was measured with the Hall probe and the measured values were converted to the proton resonance frequencies according to Eq. (1). The resulting dependence of the frequency on the x -coordinate measured for $I=2$ A is in Figure 9. As can be seen, the magnetic field is linear with a sufficient accuracy within the operational area of the probe, which is a circle with the diameter of 20 mm. Outside of this area the linearity is not so good but it does not influence our measurements.

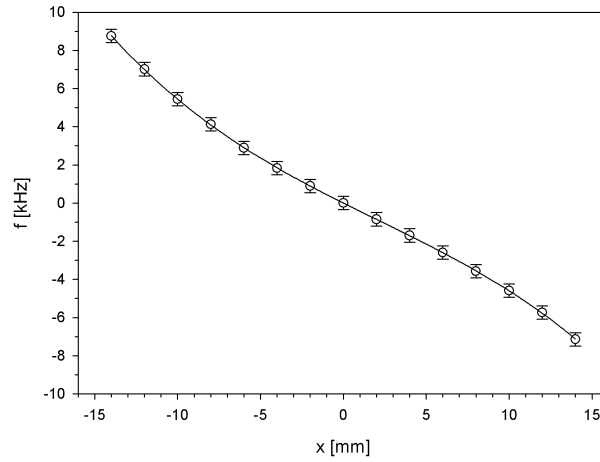


Fig. 9: Dependence of the resonance frequency ($f = \frac{\gamma}{2\pi}B_z$) on the x -coordinate, $I=2$ A. The magnetic field B_z was measured with the Hall probe.

2.2 NMR spectra in the gradient magnetic field

NMR spectra were first measured on the sample that contains two drops of water (Figure 10a). The sample was rotated with the step of 10° . When the two drops have different positions along the x -axis, there are two peaks in the NMR spectrum. When the x -coordinates of both drops equal, there is only one peak in the spectrum (see Figure 11). The dependence of resonance frequencies on the angle of the rotation is in Figure 10b. The experimental points are fitted with the curve $f(\alpha) = f_0 \pm A \sin \alpha$.

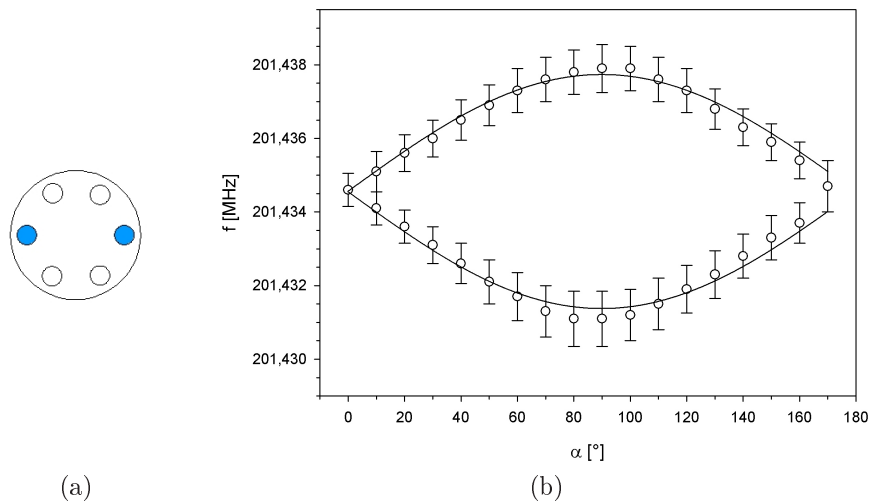


Fig. 10: (a) Sample containing two drops of water. Real dimensions: diameter 20 mm, height 10 mm. (b) Dependence of the resonance frequency on the angle α .

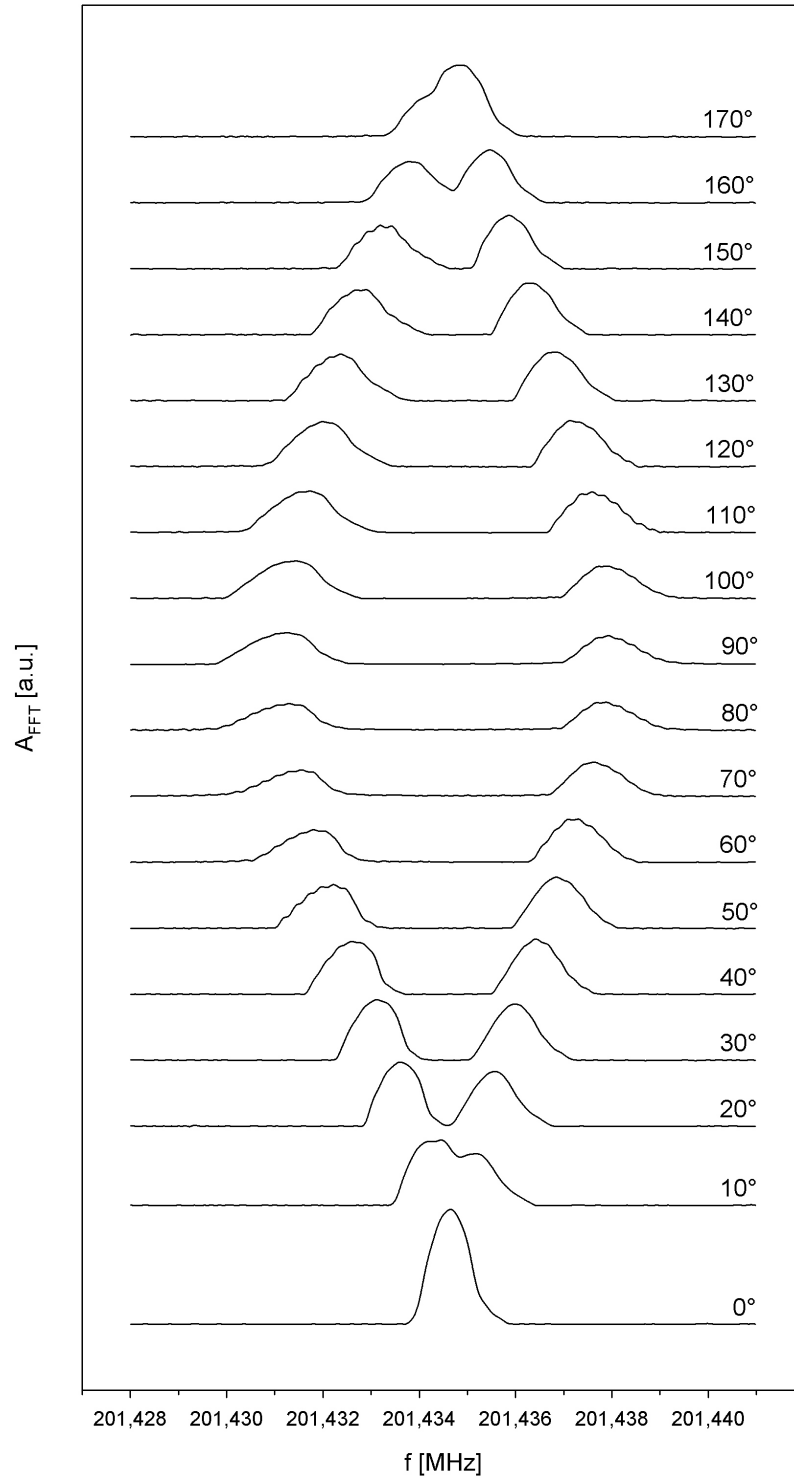


Fig. 11: NMR spectra measured on the sample (Figure 10a) in the dependence on the angle α ($\alpha = 0^\circ$ when the join of the centers of the two water containing regions is perpendicular to the gradient direction).

2.3 ρ -, T_1 - and T_2 -weighted images

To demonstrate ρ -weighted images we used a sample that contained water and partially deuterated water, which has lower proton density. The volumes of water and partially deuterated water in the measured object were the same. The object was measured by means of the spin echo pulse sequence for 18 orientations with respect to the gradient. The resulting image is in Figure 12b. Partially deuterated water looks darker which is given by its lower proton density.

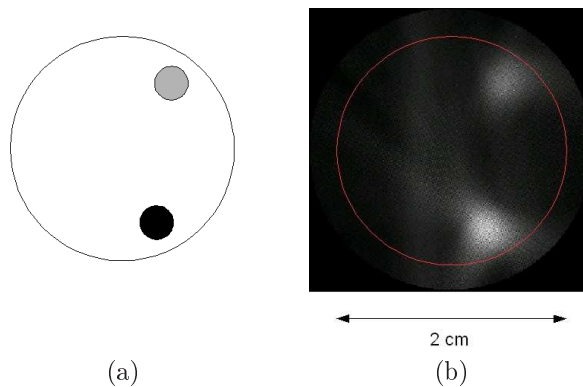


Fig. 12: ρ -weighted image. (a) Spatial structure of the measured object (black color stands for water, gray for partially deuterated water). (b) Reconstructed image.

The T_1 -weighted image was demonstrated on a sample that contained solutions of copper sulphate with two different concentrations. The spatial structure of the sample is illustrated in Figure 14a. The measurement was done by means of the inversion recovery pulse sequence for 18 orientations of the sample with different values of the delay between the 180° excitation pulse and the 90° pulse.

Looking at the spin-lattice relaxation behavior of our solutions (Figure 13), it can be seen that the signal intensity of the half-molar solution is nearly zero at $T_{Inv}=2$ ms. Therefore we set T_{Inv} to this value first. As expected, no bright area appeared in the image created by the back projection in the place where the half-molar solution was located (Figure 14b). For comparison the measurement was done on the same sample but with $T_{Inv}=10$ ms. The longitudinal component of the magnetization vector of both the molar and the half-molar solution is almost relaxed at 10 ms. In the resulting image there are bright areas in places where both solutions were located, again in agreement with the theory.

Similarly as the T_1 -weighted image also the T_2 -weighted image was demonstrated by means of an object containing solutions of copper sulphate

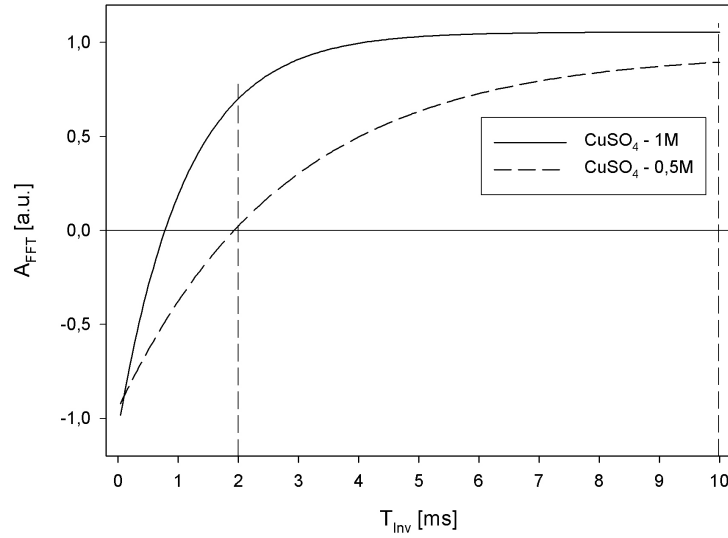


Fig. 13: Spin-lattice relaxation behavior of the molar and half-molar solution of copper sulphate.

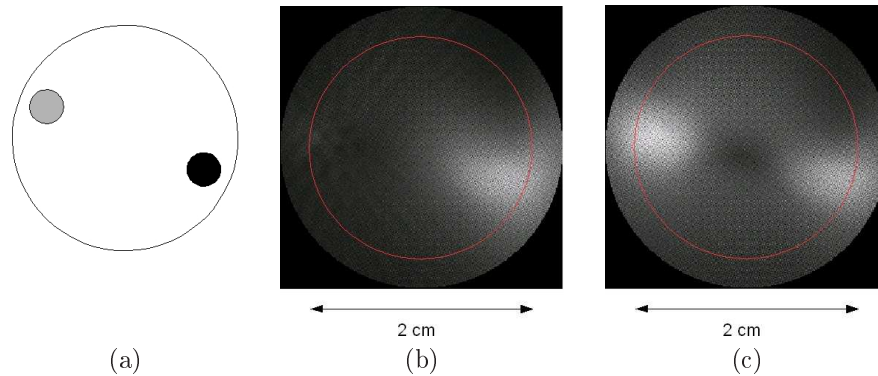


Fig. 14: T_1 -weighted image. (a) Spatial structure of the measured object (black color stands for the molar solution, gray for the half-molar solution). (b), (c) Reconstructed images – (b) $T_{Inv}=2$ ms, (c) $T_{Inv}=10$ ms.

with two different concentrations. We used a combination of the half-molar and the quarter-molar solution (Figure 16a).

The measurement was done with the delay between the 90° pulse and the 180° pulse in the spin echo pulse sequence set to 2 ms, where (as can be seen in Figure 15) the difference between the size of the transverse components of the magnetization approaches its maximum. The image in Figure 16b was created by the back projection of the set of 18 spectra measured for different orientations of the sample. As expected the areas where the half-molar solution was located appear darker.

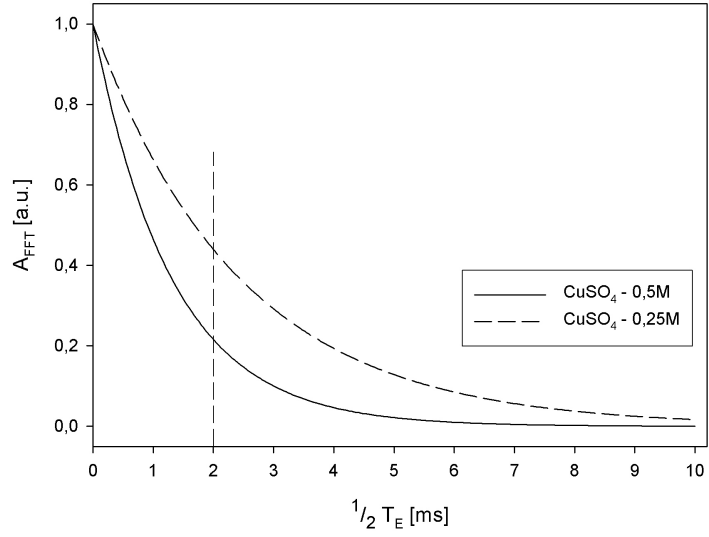


Fig. 15: Spin-spin relaxation of the half-molar and the quarter-molar solution of copper sulphate.

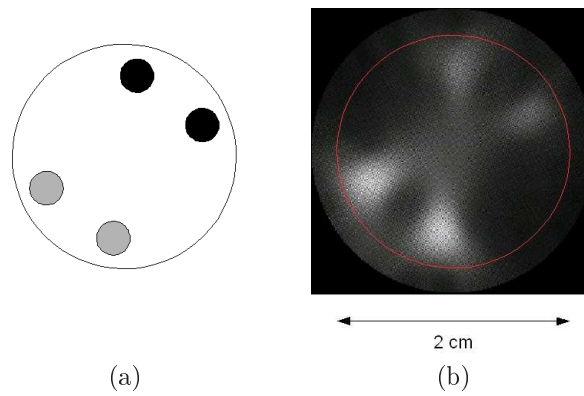


Fig. 16: T_2 -weighted image. (a) Spatial structure of the measured object (black color stands for the half-molar solution, gray for the quarter-molar solution). (b) Reconstructed image $-\frac{1}{2}T_E=2$ ms.

Conclusion

The aim of the thesis was to prepare a new experiment for the student laboratory, which should demonstrate the basic principles of the NMR imaging. The motivation was to introduce a highly up-to-date application of the nuclear magnetic resonance to students of the Faculty of Mathematics and Physics.

The new experiment should serve as an extension to an already operating experiment that demonstrates basic principles of the NMR, as the free induction decay, the spin echo, the spin-lattice and spin-spin relaxation. The new experiment offers to the students the possibility of obtaining much more specific knowledge and practical experience. They will learn how to use NMR spectra to reconstruct the shape of a measured object and how to improve contrast of the created image by means of the relaxation times T_1 and T_2 .

The thesis starts with a theoretical introduction, which is divided into two main parts. The classical description of the NMR is presented in the first part. The second part deals with the NMR imaging. It explains not only the back-projection method, used in our experimental setup, but also modern techniques of the NMR tomography as the frequency and phase encoding, and the slice selection. The improvement of contrast based on differences in the relaxation times T_1 and T_2 is also discussed.

The most important problem I should deal with was to construct the gradient coil. Its design and realization are described in detail at the beginning of the experimental part of the thesis. Another important task was to prepare the computer program for processing NMR spectra and creating images. A successful solution of these two tasks was a necessary condition for further work.

The thesis then contains the description of the NMR spectrometer that was used for measuring. The spectrometer was in operation already before the start of my PhD studies but it was several times upgraded (both hardware and software) during my work.

The last task was to choose convenient samples, measure their relaxation times and NMR spectra. These spectra were processed in order to reconstruct the shape of measured objects. We succeeded in creating not only ρ -weighted but also T_1 - and T_2 -weighted images.

Concrete tasks for students, an educational text and instructions for measuring are in the last chapter of the thesis. The educational text contains only those aspects of the NMR imaging that are necessary for understanding of the experiment. Students who are interested in more detailed information can find it in references at the end of the educational text.

List of publications

ČERNÁ, J.: Magnetic Resonance Imaging. WDS'03 Proceedings of Contributed Papers, Part III, 646–650, 2003.

ČERNÁ, J.: NMR Imaging – Nobelova cena za lékařství a fyziologii 2003. Pokroky matematiky, fyziky a astronomie, ročník 49 (2004), č. 1, 15–23

ŠTĚPÁNKOVÁ, H., ENGLICH, J., ŠTĚPÁNEK, J., KOHOUT, J., PFEFFER, M., ČERNÁ, J., CHLAN, V., PROCHÁZKA, V., BUNYATOVA, E.: Nuclear Spin-lattice Relaxations in Ethanol with Dissolved Tempo Radicals. Acta Physica Slovaca, vol. 56 (2006), No. 2, 141–144

References

- [1] BERNAS, M., DVOŘÁK, P., HOZMAN, J., KLÍMA, M.: Zpracování obrazové informace. Vydavatelství ČVUT, Praha 1996.
- [2] BRIGHAM, E. O.: The Fast Fourier Transform. Prentice-Hall, New Jersey 1974.
- [3] DOLEŽAL, I., ŠVÉDA, K.: Korekční cívky solenoidu pro jadernou magnetickou rezonanci. Elektrotechnický časopis 5 (1975), 377–391.
- [4] ENGLICH, J.: Pulzní metoda jaderné magnetické rezonance a její užití v MR tomografii. Pokroky matematiky, fyziky a astronomie 4 (1995), 198–207.
- [5] FREEMAN, R.: Basic Steps in High Resolution NMR. Spektrum Academic Publishers, Oxford 1997.
- [6] HORNAK, J. P.: www.cis.rit.edu/htbooks/mri/inside.htm (1996)
- [7] HORNAK, J. P.: www.cis.rit.edu/htbooks/nmr/nmr-main.htm (1997)
- [8] KONZBUL, P.: Generace a analýza korekčních magnetických polí pro NMR a MRI solenoidální magnety. Disertační práce, VUT Brno 1997.
- [9] PROSSER, V. & kol.: Experimentální metody biofyziky. Academia, Praha 1989.
- [10] RADON, J.: Über die Bestimmung von Funktionen durch ihre Integralwerte längst gewisser Mannigfaltigkeiten. Berichte Sächsische Akademie der Wissenschaften Math.-Phys. Kl. 69 (1917), 262–267.
- [11] RINCK, P. A.: Magnetic Resonance in Medicine. Blackwell Scientific Publications, Oxford 1993.
- [12] SCHILD, H. H.: MRI made easy. Schering, Berlin 1990.
- [13] SLICHTER, C. P.: Principles of Magnetic Resonance. Springer-Verlag, Berlin 1978.
- [14] WESTBROOK, C., KAUT, C.: MRI in Practice. Blackwell Science, Oxford 1993.